THE JOURNAL OF PHYSICAL CHEMISTRY C

Article

Cite This: J. Phys. Chem. C 2018, 122, 29405−29413

pubs.acs.org/JPCC

Assessing the Charge Transfer at the Cytochrome c_{553}/Graphene Interface: A Multiscale Investigation

Alicja M. Kowalska, Bartosz Trzaskowski, and Silvio Osella*

Chemical and Biological Systems Simulation Lab, Center of New Technologies, University of Warsaw, Banacha 2C, 02-097 Warsaw, Poland

Supporting Information

ABSTRACT: The creation of bio-organic interfaces, in which proteins play an active role in the transfer of charges, is becoming more and more important, considering the almost endless combinations of protein−metal interfaces and their potential use in biosensors and solar-to-fuel devices. In this work, we present a new interface consisting of cytochrome and graphene, in which the protein with its heme group plays a key role in the transport of charges to the metal. By means of multiscale computational simulations, we found four thermodynamically stable conformations of the protein on the graphene surface, and with in-depth *ab initio* calculations, we observed that the effective transfer of charge from graphene to the heme group strongly depends not only on the position of the group but also on its relative orientation with respect to graphene. A model porphyrin−graphene interface confirmed the interplay between orientation and position in the strength of the transfer of charges at the interface.

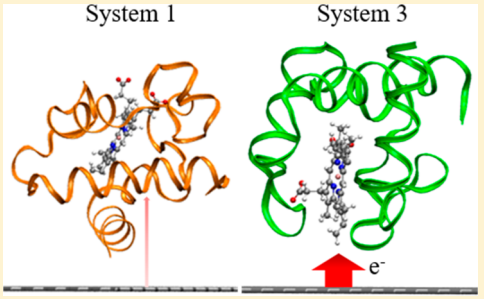

INTRODUCTION

Finding new ways to design and produce bio-organic interfaces is the key for the creation of cheap and efficient bioelectronic devices which can become a reliable alternative to the growing energy consumption, still based today on fossil fuels.[1,2] The standard procedure for the design of new bioelectronic devices is to deposit a semiconductor on noble metals or silicon and add the biological material on top of it.[3−5] An alternative route to enhance the efficiency of the device is to use a carbon-based semiconductor[6] and consider a 2D material, e.g., graphene, as the electrode. Graphene[7] is an allotrope of carbon with outstanding semimetal qualities; its delocalized $\pi-\pi$ interactions and the one-atom thickness are responsible for the presence of the overlap between the valence and conduction bands at a degeneracy high symmetry K point, creating a zero bandgap material. In addition, graphene is biocompatible,[8] possesses high mechanical strength,[9] conducts heat and electricity efficiently,[10,11] and has a charge mobility of more than 50 000 $cm^2\ V^{-1}\ s^{-1}$ under ambient conditions.[12,13] All of these properties make it a suitable candidate to create robust bio-organic interfaces. The interaction of graphene and single-walled carbon nanotubes (SWCNTs) with electron-donating or electron-withdrawing molecules, studied by means of Raman and electronic spectra, shows the strong effect of the interacting molecule on the charge transfer abilities of graphene,[14,15] as well as on the interaction energy.[16] In addition, binding energy analysis and computational studies of DNA nucleobases and nucleosides interacting with graphene and SWCNTs shed light onto the role of the different bases on the charge transfer properties of graphene, depending on the different van der Waals interaction strengths.[17,18]

One of the most interesting problems in materials science today is a controlled attachment of the biomolecule to the carbon-based electrode to create a stable system resistant to changes in temperature and humidity which enhances the electron transfer and does not require complicated synthetic processes.[19−21] The fashion in which the components of the interface are combined together has a tremendous impact on the obtained efficiency of the bioelectronic devices.[22,23] To date, three generations of biosensors have been developed.[24,25] In the first generation, the product of the reaction diffuses to the transducer and generates an electrical response; in the second, a specific mediator between the reaction and the transducer is required to cause an improved response; and in the third, the reaction itself causes a response, and no mediator or product of diffusion is directly involved in it. Immobilized biomolecules allow an efficient direct electron transfer (DET) resulting in a high current density, but their limited conformational mobility can lead to a loss of biological function. The most common solution to this problem of immobilization of biomolecules on an electrode surface is the addition of a self-assembled monolayer (SAM) between these two components. In this way, a high degree of control of the composition and thickness of the SAM lead to a fine control of the final DET generated.[26] An alternate route is to directly add an additional biomolecule to the electrode, as in third generation biosensors.[25] It has been shown that in such approaches the addition of another, small biomolecule may be

Received: October 29, 2018
Revised: November 23, 2018
Published: December 5, 2018

DOI: 10.1021/acs.jpcc.8b10517
J. Phys. Chem. C 2018, 122, 29405−29413

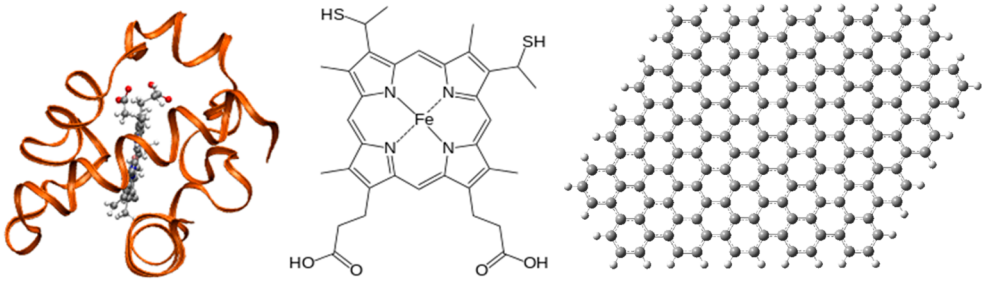

Figure 1. Schematic representation of chemical structures of the investigated components of the interfaces: cyt c_{553} model (left), the heme group responsible for the transfer of charge (center), and the graphene nanoflake (206 atoms, right) considered in the study.

beneficial in many instances. Recently, Kargul et al. used a cytochrome acting as a linker between the electrode and the light harvesting protein to allow proper flexibility of the system and, at the same time, enhance the transfer of charges to the electrode.[27] Such an approach has been successfully applied to create devices where small modifications of the linker between graphene and cytochrome have a strong impact on the final device efficiency.[5]

Cytochrome c_{553} (cyt c_{553}) is a small, water-soluble holoprotein performing a central function in the electron transport in the mitochondrial respiratory chain. This protein is also involved in important photosynthesis events such as the reduction of photo-oxidized P700 complex of PSI, playing a key role as a redox center and participating in the electron transfer. In addition, it is stable in wide pH ranges, making it applicable in organic electronics. However, electron transfer at the cyt c_{553}/solid electrode interface is usually low, with current density values on the order of μA cm^{-2}.[5] Thus, there is a need of modifying this interface in order to create electrodes which enhance the DET and at the same time preserve the electrochemical function of the protein and a good stability of the protein on the electrode. As a result, the creation of cyt c_{553}/single layer graphene (SLG) interfaces is of high interest, since this combination can on one hand take advantage of the high transfer of charges on graphene and, on the other hand, shed light on the flexibility and stability of cytochrome in such systems.

Computational studies are particularly important in investigating the DET at such interfaces, as they can give a strong insight into the mechanism and stability of the system, which is difficult to assess experimentally, leading to a rational design of possible efficient interfaces used in bioelectronics. Despite the strong interest in such systems, only few theoretical works regarding the cyt c_{553}/SLG interface have been performed up to date.[28,29] Following the approach used in the work of Janna Olmos,[5] we considered for this study cyt c_{553} as a direct linker between graphene and the light harvesting protein. In this work, we investigated the formation of a stable and efficient cyt c_{553}/SLG interface by means of multiscale simulations combining molecular dynamics simulations with DFT methods. We show that cyt c_{553} physisorbed on SLG may form stable interfaces and the direct electron transfer is strongly dependent on the position and orientation of the heme group, with a net transfer of electrons from SLG to the heme group.

COMPUTATIONAL DETAILS

Considering the complexity of the investigated systems shown in Figure 1, we have adopted a multiscale approach to assess the conformational stability as well as the electronic properties of the interfaces. The cytochrome c_{553} from the *Cyanidioschyzon merolae* (cyt c_{553}) structure was obtained using homology modeling, as implemented in Prime v.3.9,[30] with the cytochrome c_6 protein from alga *Porphyra yezoensis* as the template (PDB code: 1GDV).[31] In the first step, we applied a docking procedure to obtain the orientation of cyt c_{553} on graphene using the FTDOCK program,[32] in which both cyt and the graphene surface were considered rigid. From this analysis, we obtained a set of stable cyt c_{553}/SLG interfaces, from which we selected four with the highest docking score.

Conformational Search. The selected structures have been used as starting conformations for molecular dynamic (MD) simulations, performed using Gromacs 2016.3 software[33] and the CHARMM27 force field.[34] The force field parameters for cyt c_{553} have been modified accordingly to account for the heme−His, heme−Cys, and heme−Met interactions.[35] For all of the systems, we considered the central iron atom as Fe(II). Additionally, we used the same procedure to obtain the force-field parameters for graphene as in our previous work (see the Supporting Information).[36] In each simulation, the entire cyt c_{553}/SLG interface was surrounded by more than 6000 water molecules described by the TIP3P model and neutralized by adding Na^+ ions.

The periodic boundary box was created and oriented in such manner that the *x*- and *y*-axes were taken in the plane of the graphene monolayer, whereas the *z*-axis was perpendicular to its surface. Periodic boundary conditions were considered in all three dimensions, and the box dimension was set to $6 \times 6 \times 6$ nm^3. Electrostatic interactions were treated by the particle-mesh Ewald method,[37] and bonds were constrained by the LINCS algorithm.[38] Electrostatics and van der Waals short-range interaction cutoffs were set to 1.2 nm. Dispersion correction terms were added to account for the Verlet cutoff vdW scheme. Since the graphene is considered periodic in the *xy* plane, the NVT ensemble was used, with the Nosé−Hoover thermostat[39,40] at 300 K and a time constant of 0.5 ps. The graphene monolayer has been kept frozen along the *x*, *y*, and *z* directions during the entire simulation. The simulation time step was set to 2 fs, and the coordinates of all atoms during the simulation were saved every 1000 steps, for a total simulation time of 100 ns.

Electronic Properties. To assess the electronic properties of the systems, we performed density functional theory (DFT) calculations using the final snapshot of MD simulations for the four different cyt c_{553}/SLG interfaces. Since the system is too large for any QM approach, we considered only the heme group of the cyt c_{553} and we cut the graphene surface in such a way to accommodate the heme (i.e., without any interaction of heme with the graphene edges) and, at the same time, to avoid any zigzag edges on graphene, which can lead to a wrong

DOI: 10.1021/acs.jpcc.8b10517
J. Phys. Chem. C 2018, 122, 29405−29413

description of the properties, as reported in the literature.[41,42] We also saturated graphene carbon dangling atoms with hydrogen atoms. The schematic view of the final graphene nanoflake (GNF) obtained is reported in Figure 1.

In this part of the study, we used the Gaussian 09 suite of programs[43] and initially performed calculations using four functionals which properly describe long-range interactions; CAM-B3LYP, M062X, wB97xD, and HSE. Details of the benchmarking procedure are reported in the Supporting Information. After benchmarking, we selected the HSE functional with the 6-31G(d,p) Pople's basis set[44] for this investigation. The geometry of the heme molecule has been extracted from MD simulation, and to avoid artifacts due to the possible bending of the structure due to thermal conformational fluctuations, its geometry has been optimized at the HSE/6-31G(d,p) level of theory and then the heavy atoms superimposed to the original position by means of RMSD minimization, as found from MD simulations. Since the final heme−GNF interface for all four structures consists of more than 280 atoms, we performed only single point calculations for each structure.

Electronic Coupling. To assess the transfer integral at the studied interface, we considered the projective method.[45,46] Within this approach, the system is divided into two fragments, in which an electron or hole is localized on a fragment and can hop from one fragment to another. The fragment calculations, performed using the DFT method, follow a procedure where the orbitals of a pair of molecules (a dimer) are projected onto a basis set defined by the orbitals of each individual molecule (the fragments). The obtained set of orthogonal molecular orbital energies of the dimer is then used to express the Fock matrix as a function of the new localized basis set, which enables the formation of a block-diagonal matrix. Here, we use a local version of a software which allows the study not only of vertical couplings (i.e., HOMO−HOMO, LUMO−LUMO) but also of diagonal contributions (i.e., HOMO−1−HOMO, LUMO−LUMO+1) which might be of importance when degeneration comes into play. The system is thus split into a donor and an acceptor part, and the coupling is then calculated considering any amount of molecular orbitals from the donor and acceptor sites, with all possible contributions (vertical and diagonal coupling terms). This procedure has been applied successfully in our previous studies to different interfaces.[47,48]

RESULTS AND DISCUSSION

From the FTDOCK calculations, four different conformations of the cyt c_{553} physisorbed on graphene have been obtained (see Figure 2). The differences in their conformations are mostly due to the different distances of the heme group from graphene, which result in different interactions of the amino acids with the graphene surface (i.e., different orientations of the protein). The four resulting interfaces are dubbed systems 1, 2, 3, and 4; in system 1, the heme group is relatively far from the graphene surface (cyt c_{553} depicted in orange in Figure 2); in system 3, it is relatively close (green); and in systems 2 and 4, it is at an intermediate distance (depicted in cyan and purple).

The four selected interfaces differ in both orientation and distance of the heme group from SLG. In particular, system 3 shows the shortest distance of 0.54 nm from SLG, followed by systems 4 and 2 with distances of 1.21 and 1.02 nm, respectively, while for system 1 the minimum heme−SLG distance is 1.53 nm. The Fe(II)−SLG distance follows the same trend with the minimum values of 2.06 nm (system 1) > 1.79 nm (system 4) > 1.56 nm (system 2) > 1.27 nm (system 3). Interestingly, the cyt c_{553}−SLG distance follows a different trend, with increasing values of 0.38, 0.47, 0.49, and 0.52 nm going from system 1 to system 4, respectively.

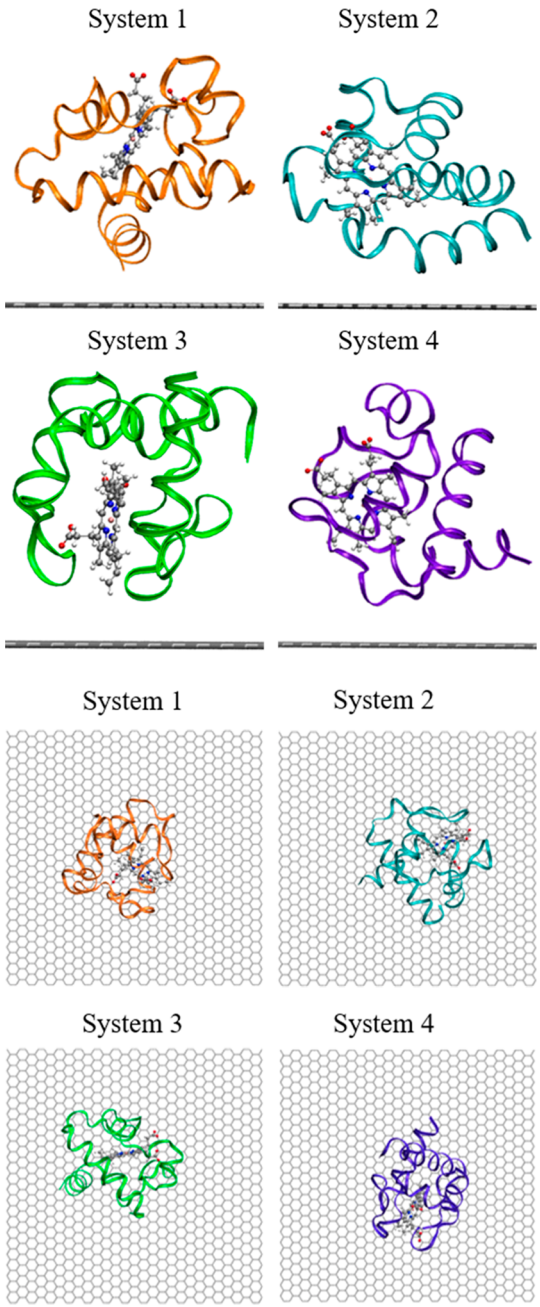

Figure 2. Stable conformations of cyt c_{553} physisorbed on a graphene surface, selected from the docking procedure; side view (top) and top view (bottom).

The four structures shown in Figure 2 have been taken as inputs for MD simulations (the final structures are reported in the Supporting Information). Since the input structures are not optimized and a long equilibration time is required, only the second half of the simulation (50−100 ns) has been considered in the MD analysis. The systems were considered equilibrated when the drift in energy was lower than 10 kJ/mol. The final structures preserve a similar orientation as observed from docking (with the heme group located at

DOI: 10.1021/acs.jpcc.8b10517
J. Phys. Chem. C 2018, 122, 29405−29413

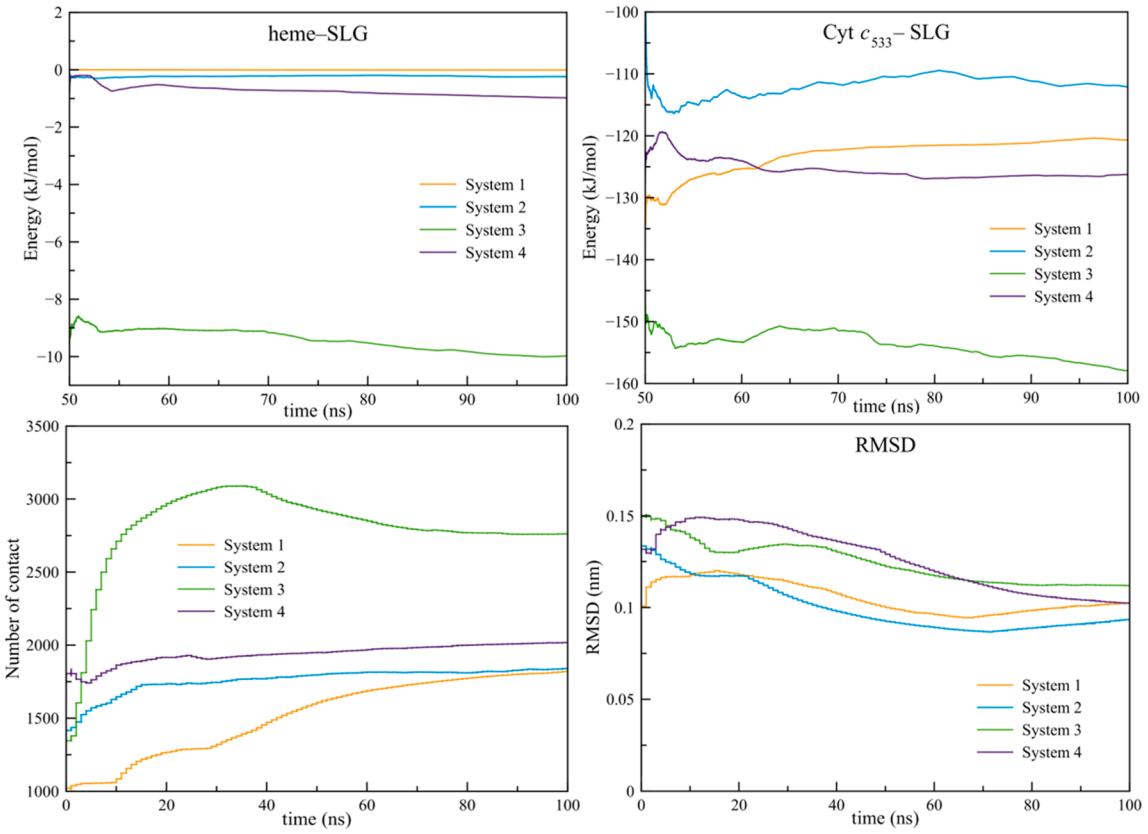

Figure 3. Running average of the van der Waals interaction energy (in kJ/mol), cyt c_{553}/SLG contact number, and RMSD analyses for the four systems. For the energy analysis, only the second half of the MD simulation is considered.

different distances and orientations from graphene) and both cyt c_{553}–SLG and heme–SLG interaction energies are analyzed, since both of these terms contribute to the overall stability of the system (Figure 3). From the heme–SLG interaction analysis, we can observe that system 3, with the shortest heme–graphene distance, has the highest average interaction energy value, of approximately −10 kJ/mol, while the other three systems show a negligible interaction energy (lower than −1 kJ/mol), directly related to the larger distance of the heme group to graphene. Similarly, the cyt c_{553}–SLG interaction is the largest for system 3, with an average value of −160 kJ/mol, while complexes 1 and 4 show values of −120 and −126 kJ/mol, respectively, and the weakest interaction was found for system 2 (−110 kJ/mol); see Table 1.

We can clearly see that the orientation of heme is only one of the factors affecting the interactions of the protein with graphene, since there are also specific hydrophobic interactions of the apolar groups of the cyt c_{553} which are facing the graphene layer which stabilize selected orientations of the protein on the surface. This is also reflected in the number of protein/SLG contacts calculated for a distance lower than 0.6 nm from the graphene monolayer. As expected, system 3 reveals the highest number of contacts, compared to the other three systems, rationalizing the stronger interaction energy calculated. Interestingly, we found that at the end of the MD simulations systems 2 and 4 had very similar properties and the RMSD analysis showed that they converged to the same conformation and orientation (see Figure S1 in the Supporting Information).

Although the cyt c_{553} is strongly absorbed on the graphene surface, its structure is very stable with final RMSD values between 0.9 and 0.11 nm. For the sake of comparison, we performed similar MD simulations of the cyt c_{553} in water without the graphene layer and obtained a RMSD value for cyt c_{553} of 0.10 nm and a radius of gyration equal to 1.13 nm. In the simulations of cyt c_{553}–SLG interfaces, the stable energy/RMSD values obtained in the second half of the simulation (50–100 ns) suggest that the presence of graphene does not distort the cyt c_{553} structure and, likely, its function. Moreover, the calculated radius of gyration has a value of 1.15 nm for all four systems, confirming only minimal changes in the conformation of the protein upon adsorption on graphene.

The calculated distance between heme and graphene from the final MD snapshots was found with the following values: 1.11 nm for system 1, 0.66 nm for system 2, 0.58 nm for system 4, and finally 0.28 nm for system 3. Considering that in a biological environment the electron transfer can occur up to a distance of 1.4 nm,[49,50] all of the analyzed structures can, in principle, be good candidates for a direct electron transfer mechanism (DET) from the cyt c_{553} to SLG or vice versa.

Table 1. Average Distances from the Protein, Heme Group, and Iron Atom to SLG and cyt c_{553}–SLG Interaction Energies Obtained from MD Simulations[a]

	system 1	system 2	system 3	system 4
cyt c_{553}–SLG distance	0.26	0.25	0.25	0.25
heme–SLG distance	1.11	0.66	0.28	0.58
Fe(II)–SLG distance	1.53	1.24	0.97	1.21
interaction energy cyt c_{553}–SLG	−120	−110	−160	−126

[a]All distances are reported in nm, while the energies are in kJ/mol.

DOI: 10.1021/acs.jpcc.8b10517
J. Phys. Chem. C 2018, 122, 29405–29413

However, for efficient DET, one should consider not only the heme−graphene distance but also the orientation of the two species involved in this process. In particular, in the case of the c_{553}/SLG system, the orientation of the heme may be a crucial parameter in assessing whether the transfer of charge is efficient. To determine the structural parameters of our interfaces, we computed the tilting angle as the angle between the plane of the heme molecule and the graphene layer plane (see Figure 4). For system 3, the heme is basically

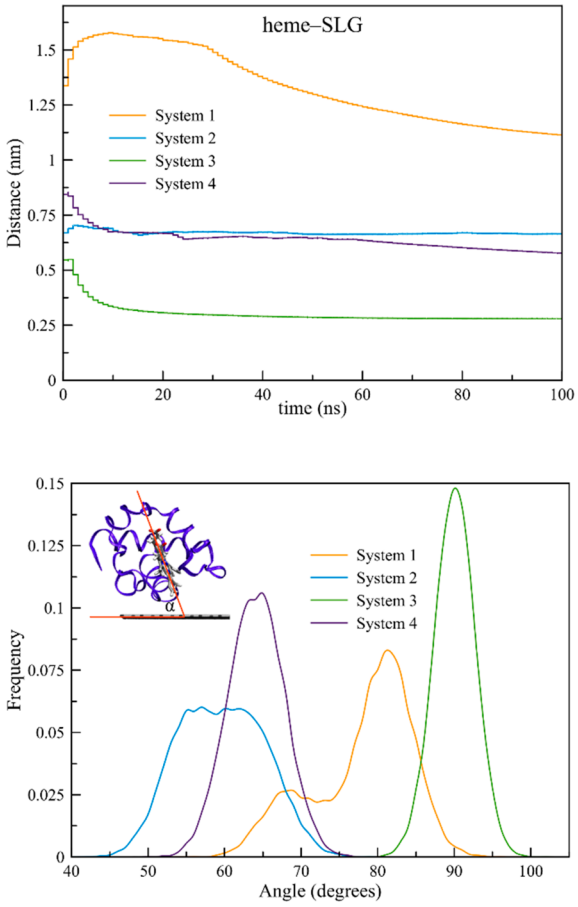

Figure 4. Heme−SLG minimum distance and angle analyses. The inset shows how the heme−SLG tilt angle has been calculated. The angle analysis has been performed for the 50−100 ns window.

perpendicular to the graphene surface, with an angle of approximately 90° and almost no fluctuations during the MD run; the other three interfaces are more flexible. In particular, system 2 has been found to have a plateau of stable tilting angle in the 55−62° window and system 4 a smaller window in between 63 and 65°. A different scenario is observed for system 1; the high degree of rotation of the cyt c_{553} and the further distance of heme to the graphene layer result in two possible different orientations of the heme on graphene: the first at around 68° and the second, more pronounced, at around 81°.

To gain insight into the transfer of charges of these interfaces, a portion of the graphene monolayer and the heme group was extracted from the MD simulations and modified as described in the Computational Details section. These four different heme/GNF interfaces are studied at the DFT level of theory and are reported in Figure 5. The calculated Fe(II)−GNF distances have values of 1.53, 1.24, 0.97, and 1.21 nm for system 1, system 2, system 3, and system 4, respectively.

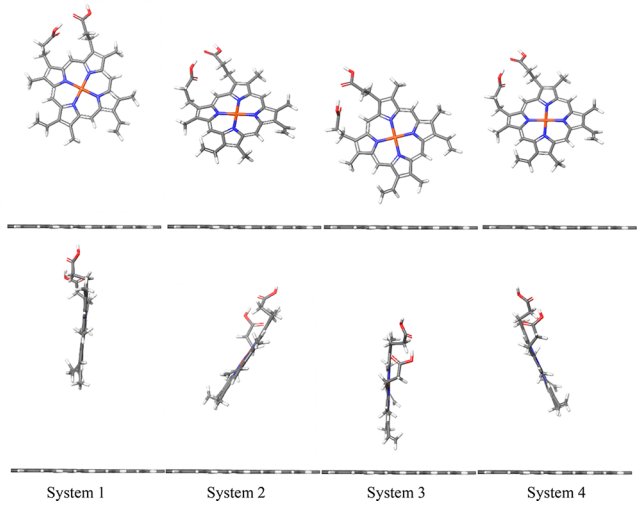

Figure 5. Frontal and side views of the four different interfaces extracted from MD simulations and used for the charge transfer calculations.

All four systems form stable interfaces, with system 3, considered as a reference at 0 eV, being the most stable, system 4 being 0.36 eV less stable and systems 1 and 2 only 0.03 eV higher in energy with respect to system 3. This data is surprising considering that in system 1 the Fe(II)−GNF distance is the longest one (1.53 nm). Accordingly, the shapes of the frontier molecular orbitals for all systems are similar, despite the different interface distances (see the Supporting Information for more details). In each case, both the highest occupied molecular orbital (HOMO) and the lowest unoccupied molecular orbital (LUMO) are localized on GNF, while HOMO−1 is localized over the heme group. As a consequence, the energy of the HOMO and LUMO is constant at around −4.40 and −3.02 eV, respectively, leading to a stable energy gap of 1.38 eV for all interfaces. On the other hand, the energy of the HOMO−1 is strongly destabilized with values of −4.64, −4.60, −4.51, and −4.40 eV going from system 1 to system 4, respectively. We can rationalize it by considering the two fragments isolated; the frontier orbitals of the GNF are close in energy, with the HOMO at −4.39 eV and the LUMO at −3.01 eV, while the same MOs for the heme groups are found at −4.73 and −2.38 eV, respectively, for the HOMO and LUMO. Thus, when the interfaces are created, the new frontier MOs are derived from the GNF, while only the HOMO−1 is derived from the heme group. Despite the similarity in electronic properties and the presence of an energy gap which is opened due to the finite size of the GNF, the differences in position and orientation of the heme group have a strong impact on the charge transfer properties of the interfaces.

The ground state charge transfer (CT) has been calculated using the electrostatic potential (ESP) charge description and results in an excess of negative charge over the heme group of −0.04, −0.01, and −0.05 |e| for systems 1, 2, and 4, respectively, with a maximum value of −0.08 |e| computed for system 3, which is substantial, considering the physisorbed nature of the interface. Interestingly, although nominally Fe(II) has a +2 charge, we found lower partial charges of 1.66 and

DOI: 10.1021/acs.jpcc.8b10517
J. Phys. Chem. C 2018, 122, 29405−29413

1.74 |e| for systems 2 and 4, respectively, and 1.92 |e| for systems 1 and 3. This different amount of charge over the iron atom can be directly related to the different orientation of the heme group on the GNF; while systems 1 and 3 are almost perpendicular to the GNF surface, with an angle close to 90°, systems 2 and 4 exhibit a strong tilting around 60°, which affect the CT ability of the whole interface. Moreover, it seems that the tilting has a stronger effect over the CT than the distance, since the iron cation in system 1 and system 3 is 1.53 and 0.97 nm from the GNF, respectively. Thus, all four different interfaces can be in thermodynamic equilibrium and take part in the charge transfer from graphene to the heme group, with stronger charge transfer for system 3, where the two components of the interface are closer. Considering that the protein has not been taken into account, these results highlight the role of the metal center in favoring the direct electron transfer (DET) from graphene to the heme group.

To gain insight into the role of the orientation of the heme group on graphene on the DET abilities, we next considered a model interface consisting of a porphyrin physisorbed on GNF, as depicted in Figure 6. First, both porphyrin and GNF

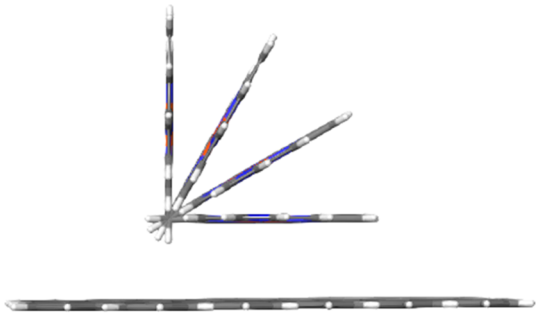

Figure 6. Model of porphyrin physisorbed on GNF. The angles considered are 0, 30, 60, and 90°, where 0° refers to the porphyrin parallel to the GNF and 90° refers to that perpendicular to GNF.

fragments are considered parallel to each other and, to assess the proper distance between the two, a scan has been performed and a minimum in energy was obtained at 3.8 Å. Next, the tilt angle between the two fragments and the normal to the GNF surface has been increased every 30°, obtaining four structures which are representative of different possible orientations of the porphyrin group on the GNF with a tilt angle of 0, 30, 60, and 90° (Figure 6).

Similarly to the heme/GNF interfaces, the electronic properties of the porphyrin/GNF system do not vary while varying the tilting of the porphyrin, since the frontier MOs are both localized over the GNF and the first orbital localized over the porphyrin fragment is HOMO−2. As a consequence, the resulting energy gap is calculated to be 1.38 eV, as obtained previously for the heme−GNF interfaces. However, in this model interface, the charge distribution shows a strong correlation with the tilt angle. In fact, when the two fragments are parallel to each other (tilt angle of 0°), a small surplus of electrons of −0.007 |e| is found on the GNF. The increase in the tilt angle is responsible for a change in behavior, with an accumulation of electrons over the porphyrin fragment which steadily increases with the magnitude of the tilt, with values of −0.011, −0.020, and −0.028 |e| for a tilting angle of 30, 60, and 90°, respectively. Thus, the CT goes from the porphyrin to the GNF when parallel, while with increasing of the tilting the CT follows the opposite direction, from GNF to the porphyrin. This result sheds light on the effect of the position of the heme group found previously; both systems 1 and 3 show a tilting angle close to 90°, which is responsible for the strong CT of electron from the GNF to the heme, while the other two systems which present a tilt of about 60° show a smaller CT in magnitude.

Finally, the transfer integral has been computed for the four interfaces investigated. The transfer integral V characterizes the strength of the electronic coupling between two adjacent molecules, which can be written as[51]

$$V = \frac{J_{AB} - \frac{1}{2}(e_A + e_B)S}{1 - S^2} \quad (1)$$

with S being the overlap matrix, e_A and e_B the diagonal elements of a Hamiltonian defined by the frontier molecular orbitals of the isolated molecules A and B, respectively, and J_{AB} the coupling of either holes or electrons, from molecule A to molecule B. Namely, for hole (electron) transfer, the HOMO and HOMO−1 (LUMO) should be considered, due to the (quasi)-degeneracy of the occupied energy levels. In the particular case of the interfaces under investigation, we consider the frontier MO degeneracy for system 4, while for all other structures only the HOMO−HOMO coupling is considered. Results of the analysis are reported in Table 2.

Table 2. Dependence of the Calculated Transfer Integrals for the Heme/GNF and Porphyrin/GNF Interfaces for Hole (h) and Electron (e) Transfer on the Different Positions and Tilting Angles[a]

interfaces	carrier	$V_{heme/GNF}$ (meV)	model interfaces	carrier	$V_{porphyrin/GNF}$ (meV)
system 1	h	6.4×10^{-8}	tilt angle 0	h	15
	e	1.5×10^{-7}		e	2.3
system 2	h	3.8×10^{-4}	tilt angle 30	h	0.29
	e	4.3×10^{-5}		e	0.51
system 3	h	1.2	tilt angle 60	h	2.7
	e	0.25		e	1.8
system 4	h	1.6×10^{-5}	tilt angle 90	h	0.94
	e	7.1×10^{-4}		e	0.29

[a]All values are given in meV.

In agreement with the analysis of the heme/GNF, we observe a negligible transfer integral for both electrons and hole carriers when the distance between heme and the GNF is substantial, higher than 0.5 nm; in particular, system 1 shows virtually no transfer for both carriers, with values lower than 10^{-8} and 10^{-7} meV; both systems 2 and 4 show an increase of transfer integral of a few orders of magnitude, up to 7.1×10^{-4} meV for electrons and 1.6×10^{-5} meV for holes; finally, system 3 presents the highest transfer integral for both carriers, with values of 1.2 meV for holes and 0.25 meV for electrons. The values computed for system 3 are comparable with commonly used material in organic photovoltaics, such as polymers.[52] Moreover, we observe a strong correlation not only between the transfer integral and the distance, which is expected to decay exponentially, but also with respect to the tilting of the heme group. In fact, system 1 and system 3 are representative of the first case (same tilt angle but different distance from GNF), while system 2 and system 4 present a similar distance from the GNF (of about 0.6 nm) but a different tilt angle, which is the main parameter responsible for

DOI: 10.1021/acs.jpcc.8b10517
J. Phys. Chem. C 2018, 122, 29405−29413

the large difference in transfer integral ability. Thus, the transport abilities of the interfaces are strongly dependent on both orientation and position, and slight changes in any of these parameters can lead to a strong decrease/increase of the charge transfer ability of the interface. We can then assume that, in a real device, thermodynamic effects can play a major role in determining the DET efficiency.

To shed light onto the unsolved debate of the effect of tilting of the heme group on the DET, we compute the transfer integral also on model interfaces in which the tilt angle is increased; see Table 2. As result, we obtain a strong transfer integral, on the order of 15 meV for holes and 2.3 meV for electrons, when the porphyrin and GNF are parallel, while a decrease of 2 (1) orders of magnitudes for holes (electrons) is observed while increasing the tilting. However, no clear trend is found with different tilting angles; while low values of 0.29 and 0.51 meV for hole and electron transfer are found for a tilting of 30°, higher values of hole (electron) transfer of 2.8 meV (1.8 meV) are obtained for a tilting of 60°, and an intermediate situation is found for a perpendicular configuration, with hole (electron) transfer of 0.94 meV (0.29 meV). Thus, it is not trivial to define what governs the transfer integral at these interfaces; it is probably due to different values of overlap and interaction energy level alignment arising from the different tilting.

CONCLUSIONS

In this paper, we assessed the electronic properties of a novel interface consisting of cyt c_{553} physisorbed on a single layer graphene by computational calculations. By performing docking and molecular dynamic simulations, we observed the presence of at least four thermodynamically stable conformations of the cyt on graphene. The peculiarity of these interfaces is the different orientation and position of the heme group, responsible for the transfer of charges at the interface. In particular, we obtained a system with the heme very close (0.3 nm, system 3) and perpendicular to graphene, one with a relatively large distance (1.1 nm, system 1) and again perpendicular to graphene, and two intermediate complexes with the heme located at 0.6 nm away from graphene and tilted to its surface (systems 2 and 4). The four interfaces carry potential differences for the transfer of charges between heme/protein and graphene. To assess the transfer of charges, we carried *ab initio* calculations on model systems, in which the protein was neglected and only the heme group interacting with graphene was considered. We showed that in all cases there is a transfer of charge from graphene to heme in the 0.1−0.8 |e| range. This result is somehow surprising, since at longer distances the CT is expected to decay exponentially. To describe the transfer of charges in a more rigorous manner, we performed the calculation of the transfer integral, which demonstrate that the amount of charge transferred depends on the distance of the heme to graphene. Our results suggest that there is virtually no transfer for the furthest conformation, but system 3 with the heme close to graphene is a very good candidate for transfer of both holes and electrons. To gain deeper insight into the effect of tilting of the heme group on the CT abilities of the interfaces, we built a porphyrin−graphene model system. From this model, we observed a net transfer of electrons from the heme to the graphene only when the two fragments were parallel to each other, while, as soon as the tilting appears, the CT was reversed, with a maximum in intensity for a perpendicular orientation. However, in this case, the transfer integral analysis did not show any clear trend, probably due to a subtle interplay of tilting and orbital overlap that govern the CT.

This study paves the way to a methodological understanding of complex bio-organic interfaces, exploiting the power of computation on complex interfaces, and it is a starting point to a more complete analysis that will clarify the different roles played by the cyt c_{553} in the transfer of charges at interfaces when a nonbiological counterpart is considered, as potential biosensors and light harvesting devices.

ASSOCIATED CONTENT

Supporting Information

The Supporting Information is available free of charge on the ACS Publications website at DOI: 10.1021/acs.jpcc.8b10517.

Snapshots from MD simulations, details of the force-field used, and molecular orbitals analysis (PDF)

AUTHOR INFORMATION

Corresponding Author

*E-mail: s.osella@cent.uw.edu.pl.

ORCID

Silvio Osella: 0000-0001-8541-1914

Notes

The authors declare no competing financial interest.

ACKNOWLEDGMENTS

S.O. acknowledges the financial support from the Polish National Science Center, grant UMO-2015/19/P/ST4/03636 (POLONEZ 1) for the funding from the European Union's Horizon 2020 research and innovation program under the Marie Skłodowska-Curie Grant Agreement No. 665778. The calculations were partially performed at the Interdisciplinary Centre for Mathematical and Computational Modelling (ICM, University of Warsaw) under the GA69-26 and GA73-16 computational grants.

REFERENCES

(1) Babadi, A. A.; Bagheri, S.; Hamid, S. B. A. Progress on implantable biofuel cell: Nano-carbon functionalization for enzyme immobilization enhancement. *Biosens. Bioelectron.* **2016**, *79*, 850−860.

(2) Karimi, A.; Othman, A.; Uzunoglu, A.; Stanciu, L.; Andreescu, S. Graphene based enzymatic bioelectrodes and biofuel cells. *Nanoscale* **2015**, *7*, 6909−6923.

(3) Savin, H.; Repo, P.; von Gastrow, G.; Ortega, P.; Calle, E.; Garin, M.; Alcubilla, R. Black silicon solar cells with interdigitated back-contacts achieve 22.1% efficiency. *Nat. Nanotechnol.* **2015**, *10*, 624−628.

(4) Yoshikawa, K.; Kawasaki, H.; Yoshida, W.; Irie, T.; Konishi, K.; Nakano, K.; Uto, T.; Adachi, D.; Kanematsu, M.; Uzu, H.; Yamamoto, K. Silicon heterojunction solar cell with interdigitated back contacts for a photoconversion efficiency over 26%. *Nature Energy* **2017**, *2*, 17032.

(5) Janna Olmos, J. D.; Becquet, P.; Gront, D.; Sar, J.; Dabrowski, A.; Gawlik, G.; Teodorczyk, M.; Pawlak, D.; Kargul, J. Biofunctionalisation of p-doped silicon with cytochrome c_{553} minimises charge recombination and enhances photovoltaic performance of the all solid-state photosystem I-based biophotoelectrode. *RSC Adv.* **2017**, *7*, 47854−47866.

(6) Zeng, Z.; Yin, Z.; Huang, X.; Li, H.; He, Q.; Lu, G.; Boey, F.; Zhang, H. Single-layer semiconducting nanosheets: high-yield preparation and device fabrication. *Angew. Chem., Int. Ed.* **2011**, *50*, 11093−11097.

DOI: 10.1021/acs.jpcc.8b10517
J. Phys. Chem. C 2018, 122, 29405−29413

(7) Geim, A. K.; Novoselov, K. S. The rise of graphene. *Nat. Mater.* **2007**, *6*, 183−192.
(8) Kuila, T.; Bose, S.; Khanra, P.; Mishra, A. K.; Kim, N. H.; Lee, J. H. Recent advances in graphene-based biosensors. *Biosens. Bioelectron.* **2011**, *26*, 4637−4648.
(9) Geim, A. K. Graphene: Status and prospects. *Science* **2009**, *324*, 1530−1534.
(10) Novoselov, K. S.; Geim, A. K.; Morozov, S. V.; Jiang, D.; Zhang, Y.; Dubonos, S. V.; Grigorieva, I. V.; Firsov, A. A. Electric field effect in atomically thin carbon films. *Science* **2004**, *306*, 666−669.
(11) Schwierz, F. Graphene transistors. *Nat. Nanotechnol.* **2010**, *5*, 487−496.
(12) Banszerus, L.; Schmitz, M.; Engels, S.; Dauber, J.; Oellers, M.; Haupt, F.; Watanabe, K.; Taniguchi, T.; Beschoten, B.; Stampfer, C. Ultrahigh-mobility graphene devices from chemical vapor deposition on reusable copper. *Sci. Adv.* **2015**, *1*, e1500222.
(13) Bonaccorso, F.; Sun, Z.; Hasan, T.; Ferrari, A. C. Graphene photonics and optoelectronics. *Nat. Photonics* **2010**, *4*, 611−622.
(14) Voggu, R.; Rout, C. S.; Franklin, A. D.; Fisher, T. S.; Rao, C. N. R. Extraordinary sensitivity of the electronic structure and properties of single-walled carbon nanotubes to molecular charge-transfer. *J. Phys. Chem. C* **2008**, *112*, 13053−13056.
(15) Das, B.; Voggu, R.; Rout, C. S.; Rao, C. N. R. Changes in the electronic structure and properties of graphene induced by molecular charge-transfer. *Chem. Commun.* **2008**, *0*, 5155−5157.
(16) Varghese, N.; Ghosh, A.; Voggu, R.; Ghosh, S.; Rao, C. N. R. Selectivity in the interaction of electron donor and acceptor molecules with graphene and single-walled carbon nanotubes. *J. Phys. Chem. C* **2009**, *113*, 16855−16859.
(17) Das, A.; Sood, A. K.; Maiti, P. K.; Das, M.; Varadarajan, R.; Rao, C. N. R. Binding of nucleobases with single-walled carbon nanotubes: Theory and experiment. *Chem. Phys. Lett.* **2008**, *453*, 266−273.
(18) Varghese, N.; Mogera, U.; Govindaraj, A.; Das, A.; Maiti, P. K.; Sood, A. K.; Rao, C. N. R. Binding of DNA nucleobases and nucleosides with graphene. *ChemPhysChem* **2009**, *10*, 206−210.
(19) Janna Olmos, D.; Kargul, J. A quest for the artificial leaf. *Int. J. Biochem. Cell Biol.* **2015**, *66*, 37−44.
(20) Feifel, S. C.; Stieger, K. R.; Lokstein, H.; Luxc, H.; Lisdata, F. High photocurrent generation by photosystem I on artificial interfaces composed of p-systemmodified graphene. *J. Mater. Chem. A* **2015**, *3*, 12188−12196.
(21) Feifel, S. C.; Lokstein, H.; Hejazi, M.; Zouni, A.; Lisdata, F. Unidirectional photocurrent of photosystem I on π-syst em-modified graphene electrodes: nanobionic approaches for the construction of photobiohybrid systems. *Langmuir* **2015**, *31*, 10590−10598.
(22) Kargul, J.; Janna Olmos, J. D.; Krupnik, T. Structure and function of photosystem I and its application in biomimetic solar-to-fuel systems. *J. Plant Physiol.* **2012**, *169*, 1639−1653.
(23) Gong, M.; Adhikari, P.; Gong, Y.; Wang, T.; Liu, Q.; Kattel, B.; Ching, W.-Y.; Chan, W.-L.; Wu, J. Z. Polarity-controlled attachment of cytochrome c for high-performance cytochrome c/graphene van der Waals heterojunction photoelectrodes. *Adv. Funct. Mater.* **2018**, *28*, 1704797.
(24) Wang, J. Nanomaterial-based electrochemical biosensors. *Analyst* **2005**, *130*, 421−426.
(25) Putzbach, W.; Ronkainen, N. J. Immobilization techniques in the fabrication of nanomaterial-based electrochemical biosensors: a review. *Sensors* **2013**, *13*, 4811−4840.
(26) Osella, S.; Kiliszek, M.; Harputlu, E.; Unlu, C. G.; Ocakoglu, K.; Kargul, J.; Trzaskowski, B. Controlling the charge transfer flow at the graphene/pyrene−nitrilotriacetic acid interface. *J. Mater. Chem. C* **2018**, *6*, 5046−5054.
(27) Kiliszek, M.; Harputlu, E.; Szalkowski, M.; Kowalska, D.; Unlu, C. G.; Haniewicz, P.; Abram, M.; Wiwatowski, K.; Niedziółka-Jönsson, J.; Maćkowski, S.; Ocakoglu, K.; Kargul, J. Orientation of photosystem I on graphene through cytochrome c553 leads to improvement in photocurrent generation. *J. Mater. Chem. A* **2018**, *6*, 18615−18626.
(28) Hu, B.; Ge, Z.; Li, X. Interface adsorption taking the most advantageous conformation for electron transfer between graphene and cytochrome C. *J. Nanosci. Nanotechnol.* **2015**, *15*, 4863−4869.
(29) Zhao, D.; Li, L.; Zhou, J. Simulation insight into the cytochrome c adsorption on graphene and graphene oxide surfaces. *Appl. Surf. Sci.* **2018**, *428*, 825−834.
(30) Jacobson, M. P.; Friesner, R. A.; Xiang, Z.; Honig, B. on the role of crystal packing forces in determining protein sidechain conformations. *J. Mol. Biol.* **2002**, *320*, 597−608.
(31) Yamada, S.; Park, S.-Y.; Shimizu, H.; Koshizuka, Y.; Kadokura, K.; Satoh, T.; Suruga, K.; Ogawa, M.; Isogai, Y.; Nishio, T.; Shiro, Y.; Oku, T. Structure of cytochrome c6 from the red alga Porphyra yezoensis at 1.57 Å resolution. *Acta Crystallogr., Sect. D: Biol. Crystallogr.* **2000**, *56*, 1577−1582.
(32) Katchalski-Katzir, E.; Shariv, I.; Eisenstein, M.; Friesem, A. A.; Aflalo, C.; Vakser, I. A. Molecular surface recognition: determination of geometric fit between proteins and their ligands by correlation techniques. *Proc. Natl. Acad. Sci. U. S. A.* **1992**, *89*, 2195−2199.
(33) Abraham, M. J.; Murtola, T.; Schulz, R.; Páll, S.; Smith, J. C.; Hess, B.; Lindahl, E. GROMACS: High performance molecular simulations through multi-level parallelism from laptops to supercomputers. *SoftwareX* **2015**, *1-2*, 19−25.
(34) Mackerell, A. D., Jr Empirical force fields for biological macromolecules: overview and issues. *J. Comput. Chem.* **2004**, *25*, 1584−604.
(35) Kaszuba, K.; Postila, P. A.; Cramariuc, O.; Sarewicz, M.; Osyczka, A.; Vattulainen, I.; Róg, T. Parameterization of the prosthetic redox centers of the bacterial cytochrome bc 1 complex for atomistic molecular dynamics simulations. *Theor. Chem. Acc.* **2013**, *132*, 1370−1383.
(36) Osella, S.; Minoia, A.; Beljonne, D. Combined molecular dynamics and density functional theory study of azobenzene-graphene interfaces. *J. Phys. Chem. C* **2016**, *120*, 6651−6658.
(37) Darden, T.; York, D.; Pedersen, L. Particle mesh Ewald: An N·log(N) method for Ewald sums in large systems. *J. Chem. Phys.* **1993**, *98*, 10089−10092.
(38) Hess, B.; Bekker, H.; Berendsen, H. J. C.; Fraaije, J. LINCS: A linear constraint solver for molecular simulations. *J. Comput. Chem.* **1997**, *18*, 1463−1472.
(39) Nose, S. A unified formulation of the constant temperature molecular-dynamics methods. *J. Chem. Phys.* **1984**, *81*, 511−519.
(40) Hoover, W. G. Canonical dynamics: Equilibrium phase-space distributions. *Phys. Rev. A: At., Mol., Opt. Phys.* **1985**, *31*, 1695−1697.
(41) Bai, J.; Huang, Y. Fabrication and electrical properties of graphene nanoribbons. *Mater. Sci. Eng., R* **2010**, *70*, 341−353.
(42) Nakada, K.; Fujita, M.; Dresselhaus, G.; Dresselhaus, M. S. Edge state in graphene ribbons: nanometer size effect and edge shape dependence. *Phys. Rev. B: Condens. Matter Mater. Phys.* **1996**, *54*, 17954−17961.
(43) Vreven, T.; Montgomery, J. A., Jr.; Peralta, J. E.; Ogliaro, F.; Bearpark, M.; Heyd, J. J.; Brothers, E.; Kudin, K. N.; Staroverov, V. N.; Kobayashi, R. *Gaussian 09*, revision D.1; Gaussian, Inc.: Wallingford, CT, 2009.
(44) Hariharan, P. C.; Pople, J. The influence of polarization functions on molecular orbital hydrogenation energies. *Theoret. Chim. Acta* **1973**, *28*, 213−222.
(45) Kirkpatrick, J. An approximate method for calculating transfer integrals based on the ZINDO hamiltonian. *Int. J. Quantum Chem.* **2008**, *108*, 51−56.
(46) Baumeier, B.; Kirkpatrick, J.; Andrienko, D. Density-functional based determination of intermolecular charge transfer properties for large-scale morphologies. *Phys. Chem. Chem. Phys.* **2010**, *12*, 11103−11113.
(47) Musumeci, C.; Osella, S.; Ferlauto, L.; Niedzialek, D.; Grisanti, L.; Bonacchi, S.; Jouaiti, A.; Milita, S.; Ciesielski, A.; Beljonne, D.; Hosseini, M. W.; Samorì, P. Influence of the supramolecular order on the electrical properties of 1D coordination polymers based materials. *Nanoscale* **2016**, *8*, 2386−2394.

DOI: 10.1021/acs.jpcc.8b10517
J. Phys. Chem. C 2018, 122, 29405−29413

(48) Döbbelin, M.; Ciesielski, A.; Haar, S.; Osella, S.; Bruna, M.; Minoia, A.; Grisanti, L.; Mosciatti, T.; Richard, F.; Prasetyanto, E. A.; De Cola, L.; Palermo, V.; Mazzaro, R.; Morandi, V.; Lazzaroni, R.; Ferrari, A. C.; Beljonne, D.; Samorì, P. Light-enhanced liquid-phase exfoliation and current photoswitching in graphene−azobenzene composites. *Nat. Commun.* **2016**, *7*, 11090.
(49) Gray, H. B.; Winkler, J. R. Long-range electron transfer. *Proc. Natl. Acad. Sci. U. S. A.* **2005**, *102*, 3534−3539.
(50) Sjulstok, E.; Olsen, J. M. H.; Solov'yov, I. A. Quantifying electron transfer reactions in biological systems: what interactions play the major role? *Sci. Rep.* **2016**, *5*, 18446.
(51) Valeev, E. F.; Coropceanu, V.; da Silva Filho, D. A.; Salman, S.; Bredas, J.-L. Effect of electronic polarization on charge-transport parameters in molecular organic semiconductors. *J. Am. Chem. Soc.* **2006**, *128*, 9882−9886.
(52) Brédas, J.-L.; Beljonne, D.; Coropceanu, V.; Cornil, J. Charge-transfer and energy-transfer processes in π-conjugated oligomers and polymers: a molecular picture. *Chem. Rev.* **2004**, *104*, 4971−5004.

DOI: 10.1021/acs.jpcc.8b10517
J. Phys. Chem. C 2018, 122, 29405−29413